Metformin protects trabecular meshwork against oxidative injury via activating integrin/ROCK signals

Lijuan Xu, Xinyao Zhang, Yin Zhao, Yang Cao, Yuanbo Liang *

Author Affiliations:

National Clinical Research Center for Ocular Diseases; The Eye Hospital of Wenzhou Medical University; Glaucoma Research Institute of Wenzhou Medical University, Zhejiang, China

*** Corresponding Author:** Yuanbo Liang, PhD

National Clinical Research Center for Ocular Diseases; The Eye Hospital of Wenzhou Medical University; Glaucoma Research Institute of Wenzhou Medical University, Wenzhou 325027, Zhejiang, China

E-mail address: yuanboliang@126.com

Abstract:

Background: This study aimed to investigate the protective effect of metformin on the trabecular meshwork (TM) and explore its molecular mechanisms *in vivo* and *in vitro*.

Methods: Ocular hypertension (OHT) mouse models were induced with dexamethasone (DEX) and further treated with metformin to determine its IOP lowering effect. Cultured human TM cells (HTMC) were pre-stimulated with tert-butyl hydroperoxide (tBHP) to induce oxidative damage and then supplemented with metformin for another 24 h. The expression of fibrotic markers and integrin/ROCK signals, including α-SMA, TGF-β, fibronectin, F-actin, integrin beta 1, Rho-associated kinase (ROCK)1/2, AMP-activated protein kinase (AMPK), myosin light chain 1 (MLC 1), and F-actin were determined by western blotting (WB) and immunofluorescence (IF). Reactive oxygen species (ROS) content was analysed using flow cytometry (FCM).

Results: Administration of metformin reduced the elevated IOP and alleviated the fibrotic activity of aqueous humour outflow in OHT models. Additionally, metformin rearranged the disordered cytoskeleton in the TM both *in vivo* and *in vitro*. Furthermore, metformin significantly inhibited ROS production and activated integrin/ROCK signalling induced by tBHP in HTMC.

Conclusion: Metformin reduced the elevated IOP in steroid-induced OHT mouse models and exerted its protective effects against oxidative injury by regulating cytoskeleton remodelling through the integrin/ROCK pathway. This study provides new insights into metformin use and preclinical evidence for the potential treatment of primary open-angle glaucoma.

Keywords: primary open-angle glaucoma, trabecular meshwork, cytoskeleton remodelling, metformin

Funding: This work was supported by the Key R&D Program of Zhejiang (2022C03112), Leading Scientific and Technological Innovation Talents in Zhejiang Province (2021R52012), National Key R&D Program of China (2020YFC2008200), Zhejiang Provincial National Science Foundation of China (LQ18H120010), Key

Innovation and Guidance Program of the Eye Hospital, School of Ophthalmology & Optometry, Wenzhou Medical University (YNZD 2201903), and the Wenzhou Municipal Technological Innovation Program of High-level Talents (No. 604090352/577).

Introduction

Intraocular pressure (IOP) elevation, predominantly resulting from increased resistance to aqueous humour outflow (AHO), is a major risk factor for primary open-angle glaucoma (POAG) deterioration (*Casson, et al.,2012*; *Wu, et al.,2020*). The only proven method is IOP lowering (*Richter and Coleman,2016*). According to Bill and his colleagues (*Bill and Hellsing,1965*; *Bill and Svedbergh,1972*), up to 80% aqueous humour is drained via conventional trabecular meshwork (TM) pathway; however, the available anti-glaucoma medications mostly act on sites other than TM and have limited efficiency. Therefore, polypharmacy has become increasingly prevalent, coupled with an increasing economic burden on society and patients (*Wu, et al.,2020*).

IOP elevation is associated with TM stiffness (*Alvarado, et al.,1984*; *Heijl, et al.,2002*; *Johnstone, et al.,2021*). Theoretically, TM-targeting drugs are potentially effective in lowering IOP caused by diseased TM. Integrin and Rho-associated protein kinase (ROCK) play pivotal roles in cytoskeleton formation and maintenance (*Tan, et al.,2020*; *Yemanyi, et al.,2020*) and ROCK inhibitor (ROCKi) can decrease actomyosin contraction and actin crosslinking (*Liu, et al.,2021*). ROCKi is the only drug that directly targets conventional outflow function (*Aga, et al.,2008*; *Rao, et al.,2001*; *Ren, et al.,2016*). It alters the architecture of AHO and expands the juxtacanalicular connective tissue region. Currently, the clinically available ROCKi include Y-27632 and ripasudil. However, the costs of Y-27632 and ripasudil are as high as 300 $ (2.5 mL) and 209 $ (5 mL), respectively. Moreover, they have not yet been approved for use in China. Considering that China is a developing country with the largest population in the world, it is urgent to explore novel TM-targeting drugs with characteristics of efficiency and lower prices, which are appropriate for our nation.

Metformin (MET), an oral biguanide insulin-sensitising drug, is the most widely used treatment for type 2 diabetes mellitus (DM) (*Foretz, et al.,2014*). It is a multifunctional drug (*Rangarajan, et al.,2018*; *Zhao, et al.,2021*). Recent studies by Lin et al. (*Lin, et al.,2015*) and Maleskic et al. (*Maleskic, et al.,2017*) found that

metformin reduced the risk of open-angle glaucoma (OAG) in patients with DM, and this effect persisted even after controlling for glycated haemoglobin. However, this effect was not observed with other hypoglycaemic medications (insulin, sulfonylureas, thiazolidinediones, and meglitinides), suggesting that the protective effect of MET on glaucoma goes beyond glycaemic improvement. However, the precise mechanisms involved remain unclear.

Excessive reactive oxygen species (ROS) in TM play an important role in the disruption of cytoskeletal integrity and apoptosis (*Hu, et al.,2017*), leading to pathological alterations in AHO and subsequent IOP rise (*Babizhayev and Bunin,1989*; *Sacca, et al.,2016*). To investigate the role of metformin in damaged TM cells and ocular hypertension (OHT) mouse models, we used tert-butyl hydroperoxide (tBHP) to induce oxidative damage in TM cells (*Tang, et al.,2013*; *Wang, et al.,2021*) and topical glucocorticoids to create OHT mouse models (*Li, et al.,2021*). The results showed that metformin protected against cytoskeletal destruction in TM by enhancing the integrin/ROCK pathway and alleviated elevated IOP in steroid-induced OHT mouse models.

Results

Steroid-induced OHT in mouse

A steroid-induced OHT mouse model was successfully established in this study. The baseline IOP did not differ between DEX-treated and PBS vehicle eyes; however, starting at day 10, IOP was significantly elevated in DEX treated eyes ($p < 0.05$, Figure 1A) and stabilised at day 21. There were no significant differences in the initial and final levels of body weight (BW) between the two groups (Figure 1B). Approximately 87.5% DEX-treated eyes had elevated IOP after 21 days of steroid induction with the averaged increased magnitude of 2.73±2.21 mmHg (0.3–6 mmHg). Moreover, the fibrotic markers (α-SMA and TGF-β) were obviously overexpressed in the OHT animal models ($p < 0.05$, Figure 1D-F).

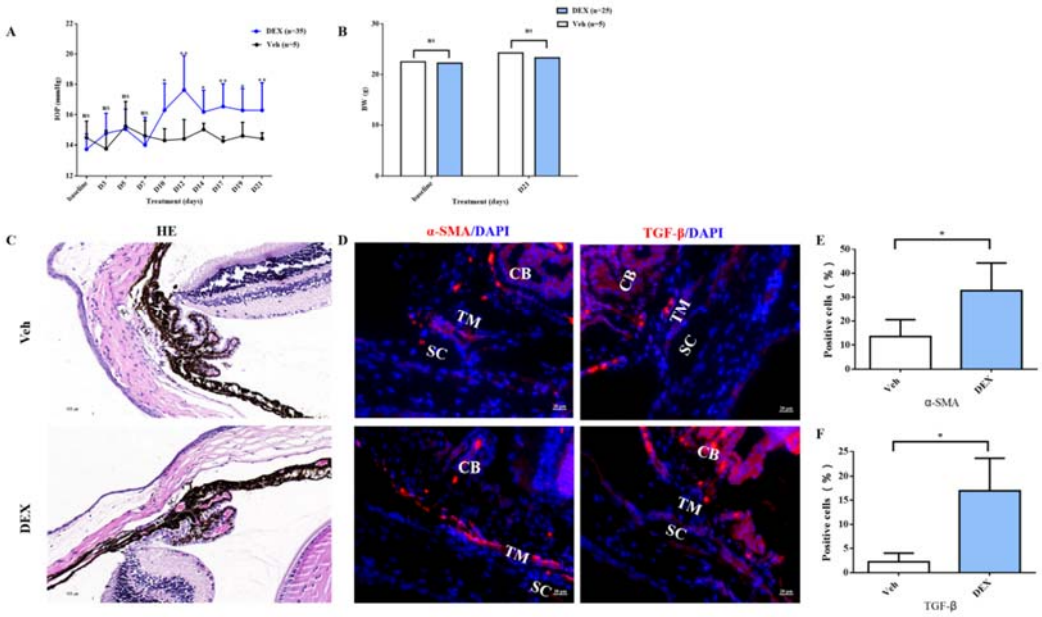

Figure 1. Topical ocular DEX induced OHT in mice. A. Elevated IOP in DEX-treated C57BL/6J mice was induced significantly at 3 weeks ($p < 0.01$). B. There was no significant change in the body weight of the DEX-treated group ($p > 0.05$). C. HE staining of OHT models. D. α-SMA and TGF-β staining in the representative OHT models. E-F. Quantification of α-SMA and TGF-β of the models. *$p < 0.05$, ns: non-significance, TM: trabecular meshwork, SC: Schlemm's canal, CB: cililary body.

Metformin effectively reversed steroid-induced OHT in mouse

To test the drug's IOP lowering effect, successfully induced OHT mouse models were randomly assigned to three groups according to different treatments for an additional 21 days consecutively: PBS eye drop (group 1), 0.3% MET eye drop (group 2), and MET oral groups (group 3). Eye drops were prescribed twice daily, whereas in group 3, a certain amount of MET for each mouse was dissolved in daily drinking water.

The experimental procedure is illustrated in Figure 2A. The IOPs after 21 days of steroid induction in all three OHT groups were similar (16.67 ± 2.28, 16.62 ± 0.81, and 15.05 ± 0.88 mmHg, respectively). After five days of MET treatment, IOPs was significantly reduced in both groups 2 and 3 ($p < 0.01$, Figure 2B). In fact, metformin almost completely reversed steroid-induced OHT, returning IOP to near baseline levels on day 5 in group 3 and on day 10 in group 2, suggesting a therapeutic role of metformin in OAG. Specific IOP values are shown in Figure 2B.

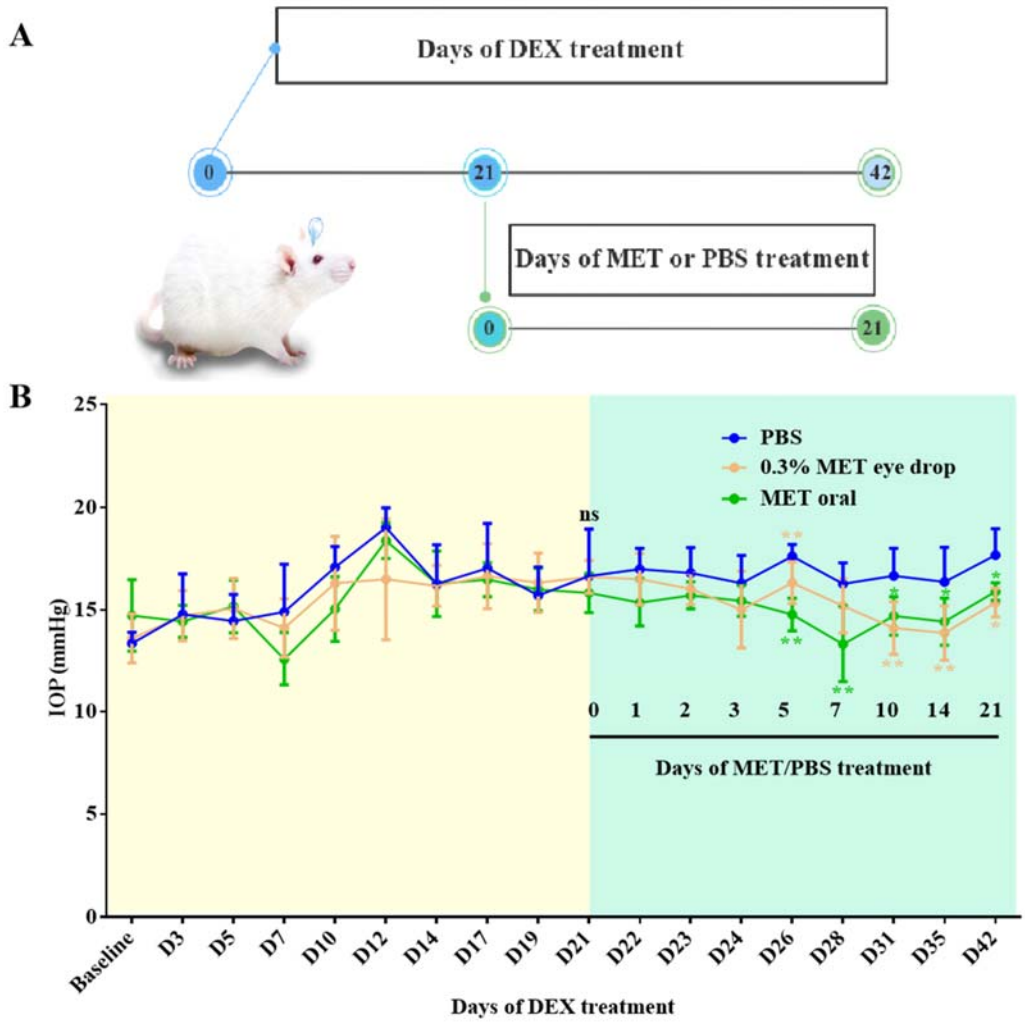

Figure 2. Effect of metformin (MET) on OHT mice model. A. Experimental process overview. B. MET effectively reversed the IOP in steroid-induced OHT mice models. *$p < 0.05$, **$p < 0.01$, ns: non-significance.

Metformin attenuated the steroid-induced TM cytoskeleton damages in vivo

As shown in Figure 3, metformin, both eye drops and oral intake, improved fibrosis and the intensity of phalloidin labelling of F-actin in TM tissue in steroid-induced OHT C57BL/6 mice (Figure 3A-B). Quantitative comparison showed a significant difference in the number of α-SMA-, TGF-β-, and fibronectin (FN)-positive TM cells between MET-treated and control mice in a time-dependent manner (Figure 3C-J). Although not statistically significant, metformin treatment promoted the cytoskeleton recovery of steroid-induced TM cell damage, as confirmed by the upregulation of

F-actin. We concluded that the IOP-lowering effect of metformin in this steroid OHT model can be largely explained by the attenuation of fibrotic alterations and rearrangement of the cell skeleton at sites of TM or trabecular outflow pathways.

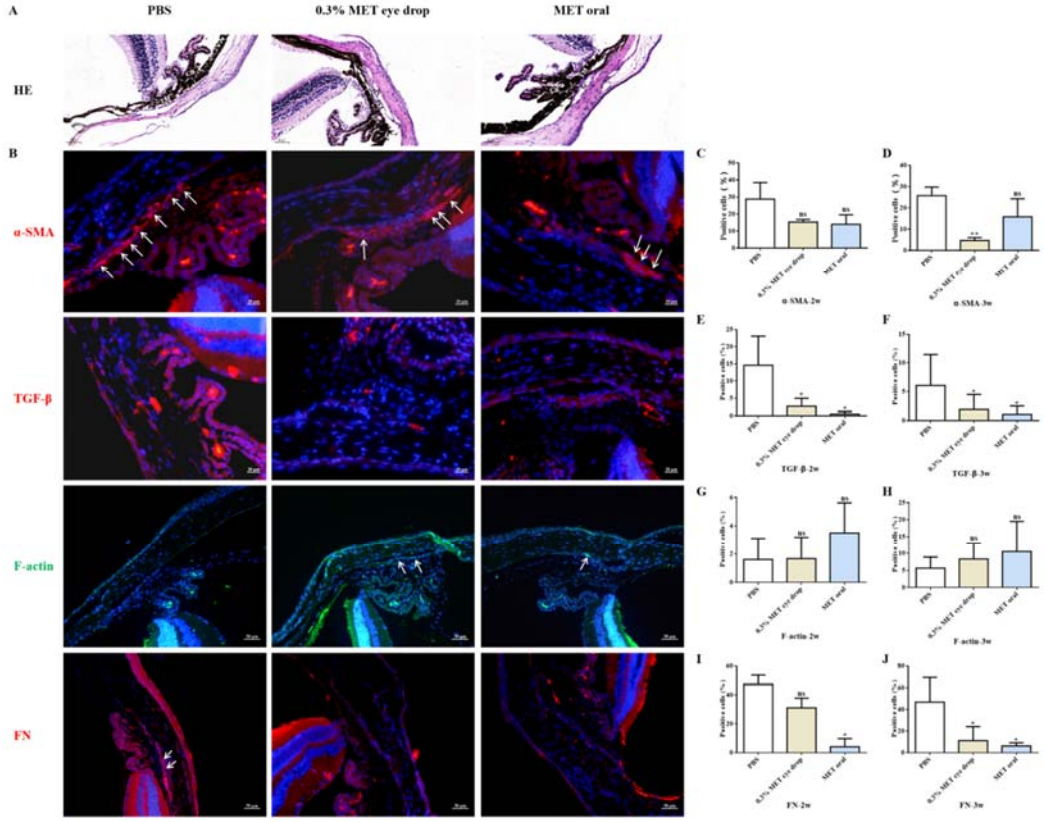

Figure 3. MET decreased the expression of fibrotic markers in steroid-induced trabecular meshwork stiffening in mice. A-B. Representative images of HE (A) and fibrotic markers (B). C-D. Quantification of α-SMA of the models after 2 weeks (C) and 3 weeks (D) of MET treatment. E-F. Quantification of TGF-β of the models after 2 weeks (E) and 3 weeks (F) of MET treatment. G-H. Quantification of F-actin of the models after 2 weeks (G) and 3 weeks (H) of MET treatment. I-J. Quantification of fibronectin (FN) of the models after 2 weeks (I) and 3 weeks (J) of MET treatment. *$p < 0.05$, **$p < 0.01$, ns: non-significance. White arrows indicate the representative positive cells.

Protection effects of metformin on TM in vitro

To test the effect of metformin on TM *in vitro*, we performed studies on HTMC. WB showed that the expression of myocilin, a glucocorticoid-inducible gene in the HTMC,

increased after DEX treatment (Figure 4B), confirming that the cells had characteristics of trabecular meshwork cells.

Higher doses (≥ 10 mM) of metformin decreased the number of HTMC, but this inhibitory effect was not evident at lower doses (< 10 mM) (Figure 4C). To verify the protective role of metformin in HTMC, cells were pre-treated with 100 μM tBHP for 1 h to induce chronic oxidative stress (*Tang, et al.,2013*), and subsequently exposed to low doses of metformin (3, 5, and 10 mM) (shortened as L-MET in this study). The results showed that L-MET significantly reversed the inhibitory effect induced by tBHP (Figure 4A, 4D).

Furthermore, cells treated with L-MET showed less intracellular ROS signals compared to the control, and 1 mM metformin reduced tBHP-induced ROS production. These results were confirmed by FCM analysis (Figure 4E-F). These results indicate that metformin reversed oxidative damage to HTMC.

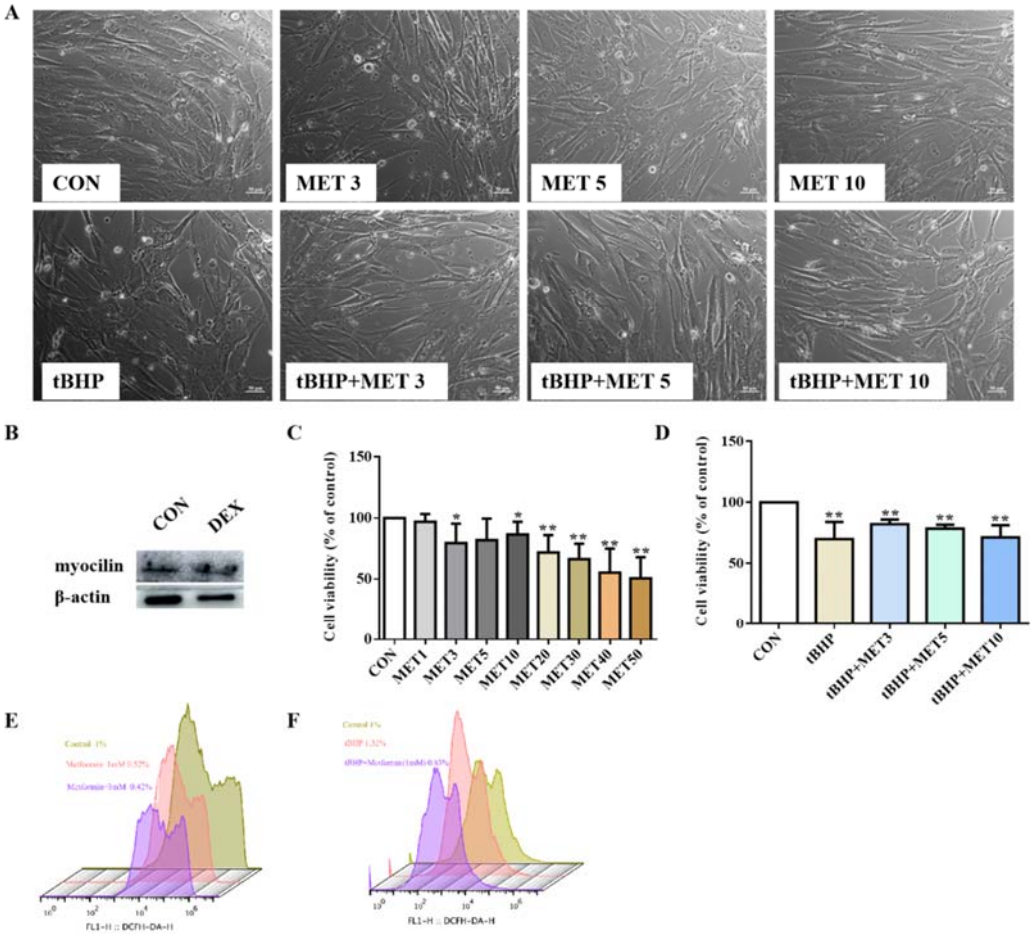

Figure 4. Low dose of metformin reversed the disarranged morphology of HTMC. A. HTMC were treated with metformin for 24 h with or without pre-treatment of tBHP for 1 h. Representative images of cell distribution and morphology photographed by inverted microscopy. B. The expression of myocilin after DEX treatment in HTMC. C-D. The relative HTMC viability after exposure to MET with different concentrations. Cell proliferation was measured using the CCK8 assay. E-F. The relative ROS levels were assayed via FCM and the results showed that metformin reduced the ROS production of HTMC induced by tBHP. $^{**}p < 0.01$. $^{*}p < 0.05$.

Metformin restored the tBHP induced cytoskeleton destruction in HTMC and activated integrin/ROCK signals

Actin filaments play key roles in cortical polarisation and asymmetric spindle localisation during phagocytosis in HTMC. F-actin was stained to determine whether actin dynamics were involved in tBHP-induced cellular dysfunction. As shown in Figure 5A, F-actin was evenly accumulated in the cytoplasm with a robust fluorescent signal in control HTMC. Exposure to L-MET did not change the morphology of HTMC as observed by inverted phase-contrast microscopy. Contrarily, HTMCs exposed to 1 h-tBHP displayed intermittent distribution of actin filaments with faded fluorescent signals. Additionally, tBHP treatment significantly destroyed HTMC, manifesting as various morphology-aberrant cells with misaligned cytoplasm. These pathological changes could be partially rescued by L-MET, implying that metformin could restore the dynamic instability from oxidative damage. Furthermore, WB results (Figure 5B-C) showed that L-MET significantly activated the integrin/ROCK pathway by upregulating integrin, ROCK, pAMPK, and F-actin, and it was more pronounced in the 3 mM and 5 mM doses.

The ultrastructures of HTMC were examined by transmission electron microscope (TEM) (Figure 6). We observed a significant reduction in the amount and density of microfilaments in the tBHP treated cells and these changes were recovered after L-MET treatment.

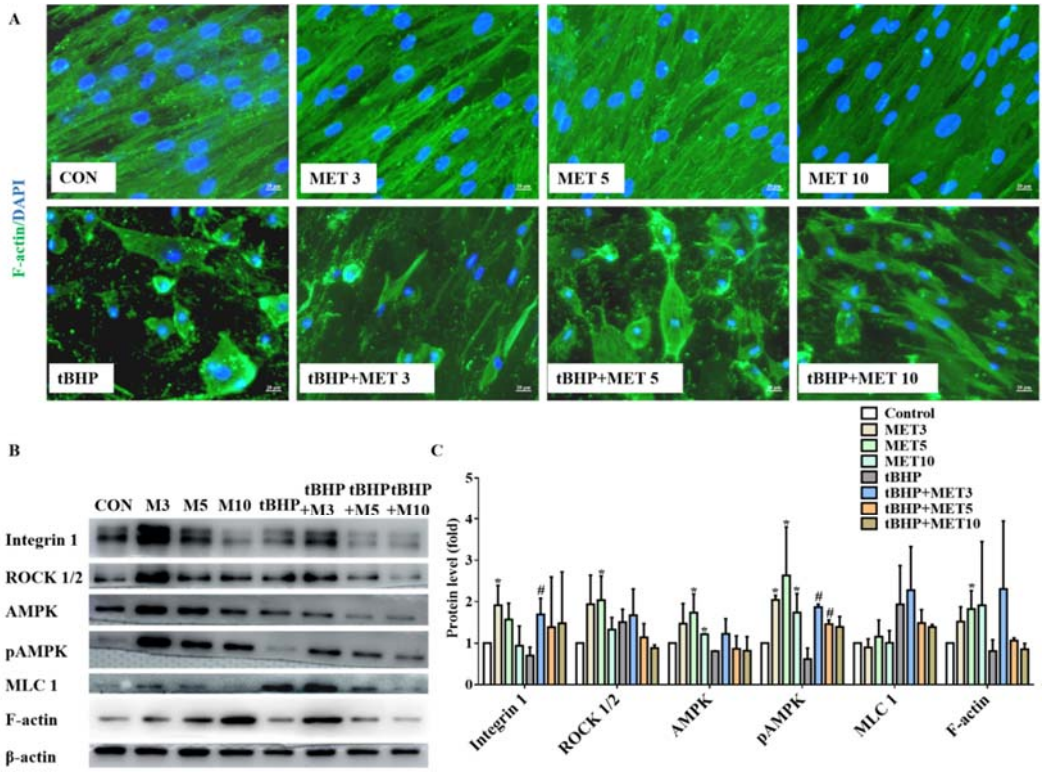

Figure 5. Metformin promoted the recovery of tBHP-induced cytoskeleton damages (A) and activated intergrin/ROCK pathway (B) in HTMC. C. The quantitative protein levels of B. * $p < 0.05$ (comparison with the control), # $p < 0.05$ (comparison with the tBHP treated group).

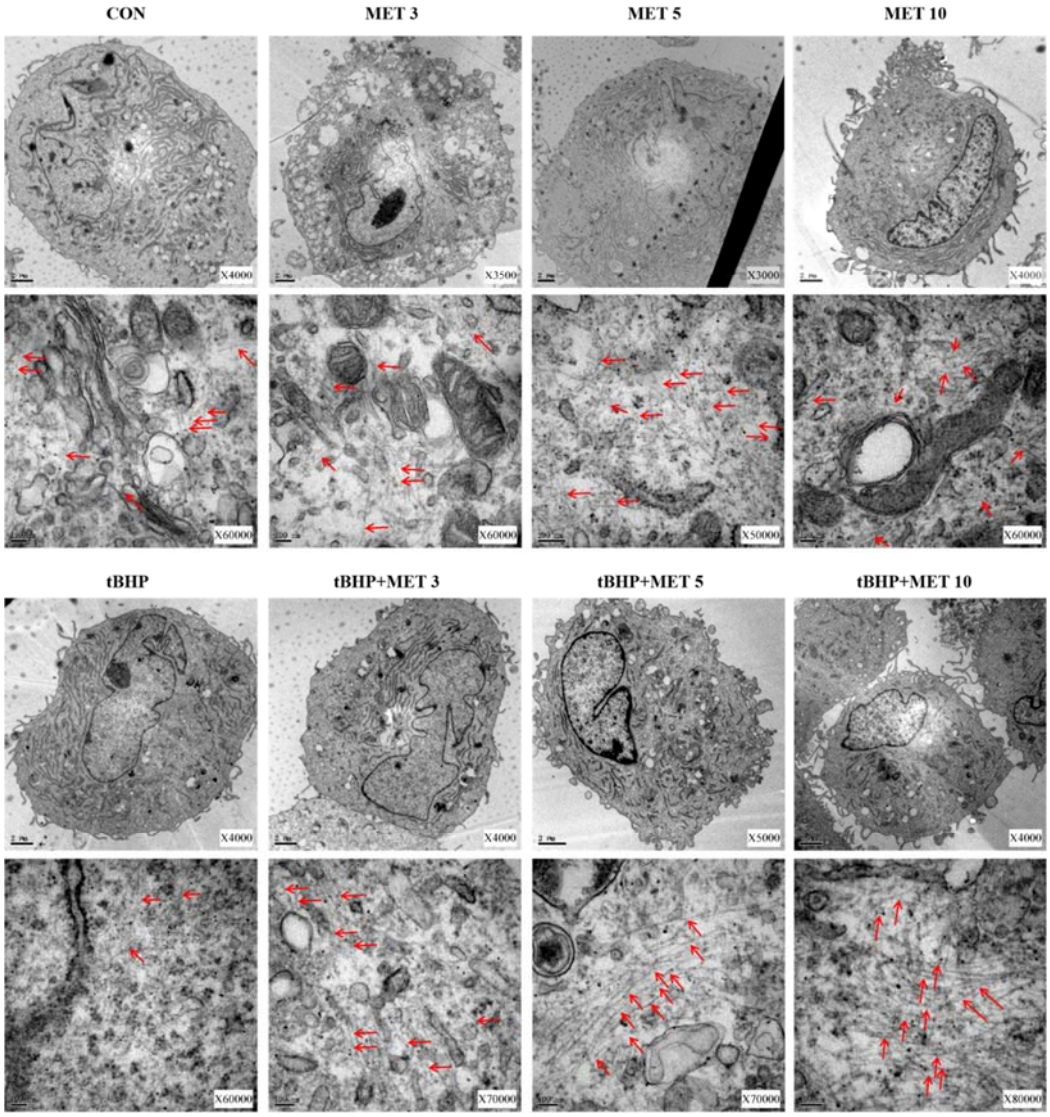

Figure 6. Metformin partially normalized the damaged microfilaments of HTMC induced by tBHP. Red arrows indicate the representative microfilaments imaged by TEM.

Discussion

The major observations of the current study were the three significant phenotypic changes induced by metformin in OHT mouse eyes and HTMC. The first was the IOP lowering effect in steroid-induced OHT mouse eyes. The second was a reversal of the skeletal destruction of TM cells, both *in vivo* and *in vitro*. Third, there was a significant decrease in the accumulation of fibrotic markers, namely α-SMA, TGF-β,

and fibronectin, in TM tissues. These results suggest a protective effect of metformin in TM, probably via promoting cytoskeleton recovery through the integrin/ROCK pathway.

Steroid-induced OHT in mice was generated (*Wang, et al.,2018*) with the characteristics of TM stiffening and elevated IOP (*Li, et al.,2019*). In line with previous studies (*Clark, et al.,2001*; *Johnson, et al.,1997*; *Johnson, et al.,1990*), our model suggested that the stiffness of AHO closely matched that of OAG in humans, including the deposition of ECM in the TM, disordered cytoskeleton, increased AHO resistance, and elevated IOP. Similar to the study by Zode et al.,*(Zode, et al.,2014)* our topical DEX elevated the IOP by 0.3–6 mmHg after 3 weeks of induction.

TM tissues play an important role in the regulation of AHO function and IOP (*Wang, et al.,2018*). TM cells have the properties of extracellular debris phagocytosis and ECM degradation. If these functions are disturbed, the balance of TM in keeping AHO free of obstructive debris is disrupted (*Last, et al.,2011*). It is noteworthy that metformin appeared to restore TM biomechanical properties in our steroid-induced OHT model after 5 days of treatment, and this restoration was accompanied by significant downregulation of ECM proteins in TM.

Moreover, as evidenced by IF and WB analyses, L-MET rearranged the disordered cytoskeleton of HTMC. This finding was supported by a study conducted by Li et al (*Li, et al.,2020*), who showed that 50 μM metformin protected oocytes against cytoskeleton destruction. Interestingly, the time course of structural changes in the TM was consistent with the observed pharmacodynamics of metformin on IOP, significantly decreasing 2 and 3 weeks of OHT because of MET treatment, which was consistent with the known effects of other ROCK regulators (*Lin, et al.,2018*; *McMurtry, et al.,2010*). Taken together, our results indicate that L-MET promotes the regeneration of abnormal HTMC and enables the recovery of TM function; this should be confirmed in future studies.

As confirmed by WB analysis, complementation with L-MET treatment upregulated integrin, pAMPK, ROCK, and F-actin signals. These *in vitro* findings indicate that metformin might elicit its protective effects through the regulation of the

integrin/ROCK pathway in HTMC. The *in vivo* observations in the OHT model again support the importance of the integrin/ROCK pathway in TM tissue protection. Generally, these signals mediate cellular biomechanical tension through actomyosin cytoskeletal tension, ECM synthesis, assembly, and degradation (*Nakajima, et al.*,*2005*; *Pattabiraman and Rao*,*2010*; *Rao, et al.*,*2001*).

Inconsistent with the previous studies indicating that the AMPK activator suppressed ROCK activity, our study revealed a novel mechanism of metformin action within which activation of both AMPK and ROCK signals sequentially upregulated F-actin expression in TM. We hypothesised that ROCK regulators might protect TM via different mechanisms, either by inhibiting ROCK signals when increased AHO resistance is attributed to TM stiffness or by activating the ROCK pathway to promote cytoskeleton formation when it is damaged. In the current study, we presumed that metformin lowered IOP through short-term changes in TM cell morphology and adhesion by regulating integrin/ROCK signalling. In addition, recovery to normal IOP prevents further TM cell loss, whereas metformin promotes the maintenance of cytoskeleton morphology and repair after injury; therefore, IOP is maintained at a normal level for an extended period.

Generally, these data emphasise the protective properties of metformin in the conventional outflow pathway, consistent with a large body of literature on other tissues (*Rangarajan, et al.*,*2018*; *Yi, et al.*,*2021*; *Zhao, et al.*,*2021*). In addition to metformin-mediated changes in ECM turnover, the observed changes in ECM composition and amount may also be due to the metformin-mediated opening of flow pathways and the consequential removal of ECM. Additionally, the observed reduction in ROS content in HTMC treated with L-MET was in line with earlier studies displaying its protective effect in several kinds of cells (*Ghasemnejad-Berenji, et al.*,*2018*; *Huang, et al.*,*2015*; *Louden, et al.*,*2014*). In any case, therapy for steroid-induced OHT, which inhibits the cycle of damage and promotes cell remodelling by restoring function to a diseased tissue, offers a potential benefit for patients.

In summary, promotion of TM cytoskeleton recovery by metformin treatment

may be an underlying mechanism for IOP reduction and AH outflow increase. A thorough investigation of the mechanisms by which cytoskeletal recovery is promoted will improve our understanding of the therapeutic mechanism of metformin. If metformin is confirmed to promote damaged cytoskeleton recovery and maintenance in the human body, it may have clear therapeutic effects on the main sites of glaucoma pathogenesis, which will broaden their application in the field of glaucoma. In conclusion, we revealed that integrin/ROCK activation reprograms metabolism in TM cells by enhancing the cytoskeleton and downregulating excessive ECM proteins.

Materials and methods

Reagent type (species) or resource	Designation	Source or reference	Identifiers	Additional information
Strain, strain background (Mus musculus)	C57BL/6J	Zhejiang Vital River Experimental Animal Technology Co. LTD (Charles River lab China)		
Cell culture	HTMC	BNCC(Shanghai, China)	338506	
Commercial assay or kit	CCK8 kit	APE BIO		
Commercial assay or kit	DCFH-DA probe	Beyotime Biotechnology, Shanghai, China		
Drug	Dexamethasone	Shanghai Macklin Biochemical Co., Ltd, China		Cell:500 nM; Animal:0.1%
Drug	Metformin	Sigma-Aldrich, St. Louis, USA		Cell:0, 1, 3, 5, 10, 20, 30, 40, and 50 mM; Animal:0.3%, 7.5 μg/day per mouse
Drug	tBHP	Damas-beta, China		Cell:100 μM

Antibody	Anti-myocilin((rabbit monoclonal)	Abcam	41552	WB(1:1000)
Antibody	Anti-integrin 1(rabbit monoclonal）	Abcam	Ab179471	WB(1:1000)
Antibody	Anti-AMPK(rabbit monoclonal）	CST	2795T	WB(1:1000)
Antibody	Anti-pAMPK(rabbit monoclonal)	CST	2535T	WB(1:1000)
Antibody	Anti-ROCK1/2(rabbi t monoclonal)	Abcam	45171	WB(1:1000)
Antibody	Anti-MLC1(rabbit monoclonal）	Abcam	Ab186436	WB(1:1000)
Antibody	Anti-F-actin(mouse monoclonal）	Abcam	Ab130935	WB(1:1000) IF（1:500）
Antibody	Anti-β-Actin(mouse monoclonal)	CST	3700S	WB(1:1000)
Antibody	Anti-α-SMA(rabbit monoclonal)	CST	19245	IF(1:500)
Antibody	Anti-TGF-β(rabbit monoclonal)	Abcam	215715	IF(1:500)
Antibody	Anti-fibronectin(rabb it monoclonal)	Abcam	Ab268020	IF(1:500)
Antibody	Anti-Rabbit IgG H&L,F(ab')2 Fragment(Alexa Fluor 594 Conjugate)	CST	8889S	IF(1:500)
Antibody	Anti-Mouse IgG H&L,F(ab')2 Fragment(Alexa Fluor 488 Conjugate)	CST	4408S	IF(1:500)
Antibody	Anti-mouse IgG,	CST	7076S	WB(1:10000)

	HRP-linked Antibody			
Antibody	Anti-rabbit IgG, HRP-linked Antibody	CST	7074S	WB(1:10000)
Other	DAPI	Beyotime Institute of Biotechnology, Shanghai, China		IF(1:500)
Software, algorithm	SPSS software	SPSS software	Version 22.0	
Software, algorithm	GraphPad Prism	GraphPad Software	Version 7.0	
Software, algorithm	ImageJ	National Institutes of Health, USA	Version 1.52a	

Animals

All the animals were treated in accordance with the principles of the Declaration of Helsinki and in compliance with the Association for Research in Vision and Ophthalmology (ARVO) Statement. All experiments were approved by the Institutional Animal Care and Use Committee of the Wenzhou Medical University (wydw2022-0209). Healthy C57BL/6J mice (age: 6–8 weeks, male) were used in this study. The mice were purchased from Zhejiang Vital River Experimental Animal Technology Co. LTD (Charles River lab China), bred/housed in clear cages, and kept in housing rooms at 21°C with a 12 h:12 h light: dark cycle.

OHT animal model and drug treatments

The animal experiments were performed in two consecutive steps. In the first step, OHT C57BL/6J mouse model was induced by topical 0.1% dexamethasone phosphate (DEX) twice daily (8–9 AM and 5–6 PM) as described previously (*Li, et al.,2021*) and sterile phosphate buffer saline (PBS) was used as a vehicle control. The second step was conducted 3 weeks after steroid induction. The successfully created OHT mice models with elevated IOP were randomly divided into three groups: control (PBS eye drops, twice daily), 0.3% MET eye drops (twice daily), and MET oral groups (7.5

μg/day for each mouse). In this step, the mice received an additional 3 weeks of supplemented drug delivery.

IOP measurements

Briefly, mice were anaesthetised using gaseous isoflurane (approximately 2 min) and topical alcaine (Alcon-couvreur n. v, Rijksweg, Puurs Belgium). IOP was measured using a rebound tonometer (icare TONOVET; Vantaa, Finland).Each recorded IOP was the average of five measurements and three IOP readings were recorded for the same eye to calculate the mean value. IOP measurements were conducted every 2–3 days (Monday, Wednesday, and Friday, between 2 PM and 3 PM).

Weight Measurement

The anaesthetised mice were gently placed on digital electronic scales (Electronic Scale, Kunshan, China) to measure their weight. The effective reading of body weight (BW) was recorded to an accuracy of 0.01 g. The BW of each mouse was calculated from the average of the three test values.

Cell culture and treatment

Human TM cells (HTMC) were purchased from BNCC (338506, Shanghai, China) and cultured in DMEM/F12 medium (Cytiva, HyClone Laboratories, Logan, Utah,) containing 10% foetal bovine serum (FBS, BI, USA) and antibiotics (100 U/mL penicillin and 100 μg/mL streptomycin, Gibco, Life Technologies Corporation, NY, USA) at 37°C and 5% CO_2. To identify the characteristics of HTMC, cells were treated with 500 nM dexamethasone (DEX) (Shanghai Macklin Biochemical Co., Ltd, China) for 7 days, and the expression of myocilin was evaluated by western blotting (WB) (*He, et al.,2019*). For drug testing, tBHP (Damas-beta, China) and metformin (Sigma-Aldrich, St. Louis, USA) were dissolved in DMEM/F12. HTMC were pre-treated with tBHP solution for 1 h to induce oxidative damage, followed by 24-h incubation in normal culture medium containing metformin at certain concentrations.

Cell viability

Cell viability was measured using the CCK8 assay kit (APE BIO), following the manufacturer's instructions. The cells were seeded in 96-well plates and exposed to increasing concentrations of metformin (0, 1, 3, 5, 10, 20, 30, 40, and 50 mM) for 24

h. The cell viability was determined by measuring the optical density at 490 nm using an absorbance microplate reader (SpectraMax 190; version 7.1.0, Molecular Devices, California, USA).

Detection of intracellular reactive oxygen species levels

Intracellular ROS levels were determined using a 2′,7′-dichlorofluorescein diacetate (DCFH-DA) probe (Beyotime Biotechnology, Shanghai, China) according to the manufacturer's instructions and a previous study (*Xu, et al.,2020*). The values were normalised to signals from the control group.

Western blotting

Cells were lysed 24 h after drug treatment as previously described (*Xu, et al.,2020*). After gel separation and membrane transfer, myocilin (Abcam), integrin 1 (Abcam), AMPK (CST), pAMPK (CST), ROCK1/2 (Abcam), MLC1 (Abcam), and F-actin (Abcam) were detected. β-Actin (CST) was used as the loading control. Western blot membranes were developed using a chemiluminescence detection system (Amersham Imager 680RGE; GE Healthcare Bio-Sciences AB, Sweden, Japan).

Histology, immunostaining and transmission electron microscope (TEM)

At the time of harvest, the mice were re-anesthetized, and the eyes were fixed in 4% paraformaldehyde overnight, embedded in paraffin or optimum cutting temperature compound in sagittal axis. The sections were incubated overnight with primary antibodies at 4°C according to the manufacturers' instructions (*Xu, et al.,2020*).α-SMA (CST), TGF-β (Abcam), F-actin (Abcam), fibronectin（Abcam）were detected. The secondary antibodies were goat anti-rabbit or anti-mouse (CST) at a 1:500 dilution. Sections were subsequently incubated with 2-(4-Amidinophenyl)-6-indolecarbamidine dihydrochloride (DAPI, Beyotime Institute of Biotechnology, Shanghai, China) for 5 min to stain the nuclei, washed, and then mounted.

The cells were fixed with 4% paraformaldehyde for 15 min, permeabilised with 0.25% Triton X-100 for 20 min, and blocked with 5% bovine serum albumin for 1 h at room temperature. After blocking, they were incubated overnight with primary antibodies at 4°C. The next day, the cells were rinsed and incubated with secondary

antibodies conjugated to Alexa Fluor (CST) for 1 h at room temperature. Fluorescent images were obtained using a confocal microscope (X-Cite Series 120, Lumen Dynamics Group Inc., Canada).

For electron microscopy studies, cells was fixed in 2.5% glutaraldehyde (Shanghai Macklin Biochemical Co., Ltd, China) and embedded in Epon resin and 80 nm sagittal thin sections were cut through iridocorneal tissues using an ultramicrotome (Power Tome-XL, RMC Products, USA). Sections were stained with uranylacetate/lead citrate and examined with a transmission electron microscope (HITACHI, H-7500).

Image analysis

Immunohistochemical images were obtained using a microscope (ECLIPSE 80i, Nikon) and analysed using the NIS-Elements Imaging Software (3.22.00; Build 700, LO, USA). For quantification, high-power fields (400× magnification) of the AHO from each model were captured. ImageJ (v1.52a, National Institutes of Health, USA) was used to quantify the positively stained cells.

Statistical analysis

Data analysis was conducted using SPSS (version 22.0) software and GraphPad Prism (version 7.0). Cell-based and animal-based experiments included at least three biological replicates. Continuous data are summarised as mean±standard deviation. The Student's t-test and ANOVA were used to test the differences in continuous variables. A paired t-test was used to compare IOP changes from the baseline. Statistical significance was set at p value < 0.05.

Financial Disclosures: The authors indicate no financial conflicts of interest.

Data availability:

All data generated or analysed during this study are included in the manuscript and supporting files. Source data files have been provided for Figures 1, 2, 3, 4 and 5.

References:

Aga M, Bradley JM, Keller KE, Kelley MJ, Acott TS. 2008. Specialized podosome- or invadopodia-like

403 structures (PILS) for focal trabecular meshwork extracellular matrix turnover. *Invest Ophthalmol Vis*
404 *Sci* **49**:5353-5365. doi:10.1167/iovs.07-1666
405 Alvarado J, Murphy C, Juster R. 1984. Trabecular meshwork cellularity in primary open-angle glaucoma
406 and nonglaucomatous normals. *OPHTHALMOLOGY* **91**:564-579. doi:10.1016/s0161-6420(84)34248-8
407 Babizhayev MA, Bunin A. 1989. Lipid peroxidation in open-angle glaucoma. *Acta Ophthalmol (Copenh)*
408 **67**:371-377. doi:10.1111/j.1755-3768.1989.tb01617.x
409 Bill A, Hellsing K. 1965. Production and drainage of aqueous humor in the cynomolgus monkey
410 (Macaca irus). *Invest Ophthalmol* **4**:920-926.
411 Bill A, Svedbergh B. 1972. Scanning electron microscopic studies of the trabecular meshwork and the
412 canal of Schlemm--an attempt to localize the main resistance to outflow of aqueous humor in man. *Acta*
413 *Ophthalmol (Copenh)* **50**:295-320. doi:10.1111/j.1755-3768.1972.tb05954.x
414 Casson RJ, Chidlow G, Wood JP, Crowston JG, Goldberg I. 2012. Definition of glaucoma: clinical and
415 experimental concepts. *CLIN EXP OPHTHALMOL* **40**:341-349. doi:10.1111/j.1442-9071.2012.02773.x
416 Clark AF, Steely HT, Dickerson JJ, English-Wright S, Stropki K, McCartney MD, Jacobson N, Shepard
417 AR, Clark JI, Matsushima H, Peskind ER, Leverenz JB, Wilkinson CW, Swiderski RE, Fingert JH,
418 Sheffield VC, Stone EM. 2001. Glucocorticoid induction of the glaucoma gene MYOC in human and
419 monkey trabecular meshwork cells and tissues. *Invest Ophthalmol Vis Sci* **42**:1769-1780.
420 Foretz M, Guigas B, Bertrand L, Pollak M, Viollet B. 2014. Metformin: from mechanisms of action to
421 therapies. *CELL METAB* **20**:953-966. doi:10.1016/j.cmet.2014.09.018
422 Ghasemnejad-Berenji M, Ghazi-Khansari M, Yazdani I, Nobakht M, Abdollahi A, Ghasemnejad-Berenji
423 H, Mohajer AJ, Pashapour S, Dehpour AR. 2018. Effect of metformin on germ cell-specific apoptosis,
424 oxidative stress and epididymal sperm quality after testicular torsion/detorsion in rats. *ANDROLOGIA*
425 **50**doi:10.1111/and.12846
426 He JN, Zhang SD, Qu Y, Wang HL, Tham CC, Pang CP, Chu WK. 2019. Rapamycin Removes Damaged
427 Mitochondria and Protects Human Trabecular Meshwork (TM-1) Cells from Chronic Oxidative Stress.
428 *MOL NEUROBIOL* **56**:6586-6593. doi:10.1007/s12035-019-1559-5
429 Heijl A, Leske MC, Bengtsson B, Hyman L, Bengtsson B, Hussein M. 2002. Reduction of intraocular
430 pressure and glaucoma progression: results from the Early Manifest Glaucoma Trial. *Arch Ophthalmol*
431 **120**:1268-1279. doi:10.1001/archopht.120.10.1268
432 Hu DB, Li ZS, Ali I, Xu LJ, Fang NZ. 2017. Effect of potential role of p53 on embryo development arrest
433 induced by H2O2 in mouse. *In Vitro Cell Dev Biol Anim* **53**:344-353. doi:10.1007/s11626-016-0122-1
434 Huang Y, Yu Y, Gao J, Li R, Zhang C, Zhao H, Zhao Y, Qiao J. 2015. Impaired oocyte quality induced by
435 dehydroepiandrosterone is partially rescued by metformin treatment. *PLOS ONE* **10**:e122370.
436 doi:10.1371/journal.pone.0122370
437 Johnson D, Gottanka J, Flugel C, Hoffmann F, Futa R, Lutjen-Drecoll E. 1997. Ultrastructural changes in
438 the trabecular meshwork of human eyes treated with corticosteroids. *Arch Ophthalmol* **115**:375-383.
439 doi:10.1001/archopht.1997.01100150377011
440 Johnson DH, Bradley JM, Acott TS. 1990. The effect of dexamethasone on glycosaminoglycans of
441 human trabecular meshwork in perfusion organ culture. *Invest Ophthalmol Vis Sci* **31**:2568-2571.
442 Johnstone M, Xin C, Tan J, Martin E, Wen J, Wang RK. 2021. Aqueous outflow regulation - 21st century
443 concepts. *PROG RETIN EYE RES* **83**:100917. doi:10.1016/j.preteyeres.2020.100917
444 Last JA, Pan T, Ding Y, Reilly CM, Keller K, Acott TS, Fautsch MP, Murphy CJ, Russell P. 2011. Elastic
445 modulus determination of normal and glaucomatous human trabecular meshwork. *Invest Ophthalmol Vis*
446 *Sci* **52**:2147-2152. doi:10.1167/iovs.10-6342

Li G, Lee C, Agrahari V, Wang K, Navarro I, Sherwood JM, Crews K, Farsiu S, Gonzalez P, Lin CW, Mitra AK, Ethier CR, Stamer WD. 2019. In vivo measurement of trabecular meshwork stiffness in a corticosteroid-induced ocular hypertensive mouse model. *Proc Natl Acad Sci U S A* **116**:1714-1722. doi:10.1073/pnas.1814889116

Li G, Lee C, Read AT, Wang K, Ha J, Kuhn M, Navarro I, Cui J, Young K, Gorijavolu R, Sulchek T, Kopczynski C, Farsiu S, Samples J, Challa P, Ethier CR, Stamer WD. 2021. Anti-fibrotic activity of a rho-kinase inhibitor restores outflow function and intraocular pressure homeostasis. *ELIFE* **10**doi:10.7554/eLife.60831

Li WD, Zang CJ, Yin S, Shen W, Sun QY, Zhao M. 2020. Metformin protects against mouse oocyte apoptosis defects induced by arecoline. *Cell Prolif* **53**:e12809. doi:10.1111/cpr.12809

Lin CW, Sherman B, Moore LA, Laethem CL, Lu DW, Pattabiraman PP, Rao PV, DeLong MA, Kopczynski CC. 2018. Discovery and Preclinical Development of Netarsudil, a Novel Ocular Hypotensive Agent for the Treatment of Glaucoma. *J Ocul Pharmacol Ther* **34**:40-51. doi:10.1089/jop.2017.0023

Lin HC, Stein JD, Nan B, Childers D, Newman-Casey PA, Thompson DA, Richards JE. 2015. Association of Geroprotective Effects of Metformin and Risk of Open-Angle Glaucoma in Persons With Diabetes Mellitus. *JAMA OPHTHALMOL* **133**:915-923. doi:10.1001/jamaophthalmol.2015.1440

Liu Z, Li S, Qian X, Li L, Zhang H, Liu Z. 2021. RhoA/ROCK-YAP/TAZ Axis Regulates the Fibrotic Activity in Dexamethasone-Treated Human Trabecular Meshwork Cells. *Front Mol Biosci* **8**:728932. doi:10.3389/fmolb.2021.728932

Louden ED, Luzzo KM, Jimenez PT, Chi T, Chi M, Moley KH. 2014. TallyHO obese female mice experience poor reproductive outcomes and abnormal blastocyst metabolism that is reversed by metformin. *Reprod Fertil Dev* **27**:31-39. doi:10.1071/RD14339

Maleskic S, Kusturica J, Gusic E, Rakanovic-Todic M, Secic D, Burnazovic-Ristic L, Kulo A. 2017. Metformin use associated with protective effects for ocular complications in patients with type 2 diabetes - observational study. *Acta Med Acad* **46**:116-123. doi:10.5644/ama2006-124.196

McMurtry IF, Abe K, Ota H, Fagan KA, Oka M. 2010. Rho kinase-mediated vasoconstriction in pulmonary hypertension. *ADV EXP MED BIOL* **661**:299-308. doi:10.1007/978-1-60761-500-2_19

Nakajima E, Nakajima T, Minagawa Y, Shearer TR, Azuma M. 2005. Contribution of ROCK in contraction of trabecular meshwork: proposed mechanism for regulating aqueous outflow in monkey and human eyes. *J Pharm Sci* **94**:701-708. doi:10.1002/jps.20285

Pattabiraman PP, Rao PV. 2010. Mechanistic basis of Rho GTPase-induced extracellular matrix synthesis in trabecular meshwork cells. *Am J Physiol Cell Physiol* **298**:C749-C763. doi:10.1152/ajpcell.00317.2009

Rangarajan S, Bone NB, Zmijewska AA, Jiang S, Park DW, Bernard K, Locy ML, Ravi S, Deshane J, Mannon RB, Abraham E, Darley-Usmar V, Thannickal VJ, Zmijewski JW. 2018. Metformin reverses established lung fibrosis in a bleomycin model. *NAT MED* **24**:1121-1127. doi:10.1038/s41591-018-0087-6

Rangarajan S, Bone NB, Zmijewska AA, Jiang S, Park DW, Bernard K, Locy ML, Ravi S, Deshane J, Mannon RB, Abraham E, Darley-Usmar V, Thannickal VJ, Zmijewski JW. 2018. Metformin reverses established lung fibrosis in a bleomycin model. *NAT MED* **24**:1121-1127. doi:10.1038/s41591-018-0087-6

Rao PV, Deng PF, Kumar J, Epstein DL. 2001. Modulation of aqueous humor outflow facility by the Rho kinase-specific inhibitor Y-27632. *Invest Ophthalmol Vis Sci* **42**:1029-1037.

Rao PV, Deng PF, Kumar J, Epstein DL. 2001. Modulation of aqueous humor outflow facility by the Rho kinase-specific inhibitor Y-27632. *Invest Ophthalmol Vis Sci* **42**:1029-1037.

Ren R, Li G, Le TD, Kopczynski C, Stamer WD, Gong H. 2016. Netarsudil Increases Outflow Facility in Human Eyes Through Multiple Mechanisms. *Invest Ophthalmol Vis Sci* **57**:6197-6209. doi:10.1167/iovs.16-20189

Richter GM, Coleman AL. 2016. Minimally invasive glaucoma surgery: current status and future prospects. *Clin Ophthalmol* **10**:189-206. doi:10.2147/OPTH.S80490

Sacca SC, Gandolfi S, Bagnis A, Manni G, Damonte G, Traverso CE, Izzotti A. 2016. The Outflow Pathway: A Tissue With Morphological and Functional Unity. *J CELL PHYSIOL* **231**:1876-1893. doi:10.1002/jcp.25305

Tan J, Wang X, Cai S, He F, Zhang D, Li D, Zhu X, Zhou L, Fan N, Liu X. 2020. C3 Transferase-Expressing scAAV2 Transduces Ocular Anterior Segment Tissues and Lowers Intraocular Pressure in Mouse and Monkey. *Mol Ther Methods Clin Dev* **17**:143-155. doi:10.1016/j.omtm.2019.11.017

Tang TH, Chang CT, Wang HJ, Erickson JD, Reichard RA, Martin AG, Shannon EK, Martin AL, Huang YW, Aronstam RS. 2013. Oxidative stress disruption of receptor-mediated calcium signaling mechanisms. *J BIOMED SCI* **20**:48. doi:10.1186/1423-0127-20-48

Wang K, Li G, Read AT, Navarro I, Mitra AK, Stamer WD, Sulchek T, Ethier CR. 2018. The relationship between outflow resistance and trabecular meshwork stiffness in mice. *Sci Rep* **8**:5848. doi:10.1038/s41598-018-24165-w

Wang Q, Chen G, Zhang Q, Wang M, Wang G, Hu T. 2021. Microcystin-leucine arginine blocks vasculogenesis and angiogenesis through impairing cytoskeleton and impeding endothelial cell migration by downregulating integrin-mediated Rho/ROCK signaling pathway. *Environ Sci Pollut Res Int* **28**:67108-67119. doi:10.1007/s11356-021-15337-9

Wu A, Khawaja AP, Pasquale LR, Stein JD. 2020. A review of systemic medications that may modulate the risk of glaucoma. *Eye (Lond)* **34**:12-28. doi:10.1038/s41433-019-0603-z

Wu A, Khawaja AP, Pasquale LR, Stein JD. 2020. A review of systemic medications that may modulate the risk of glaucoma. *Eye (Lond)* **34**:12-28. doi:10.1038/s41433-019-0603-z

Xu LJ, Rong SS, Xu YS, Zheng LB, Qiu WY, Zhang X, Jiang LJ, Duan RP, Tian T, Yao YF. 2020. Anti-fibrosis potential of pirarubicin via inducing apoptotic and autophagic cell death in rabbit conjunctiva. *EXP EYE RES* **200**:108215. doi:10.1016/j.exer.2020.108215

Yemanyi F, Baidouri H, Burns AR, Raghunathan V. 2020. Dexamethasone and Glucocorticoid-Induced Matrix Temporally Modulate Key Integrins, Caveolins, Contractility, and Stiffness in Human Trabecular Meshwork Cells. *Invest Ophthalmol Vis Sci* **61**:16. doi:10.1167/iovs.61.13.16

Yi H, Huang C, Shi Y, Cao Q, Chen J, Chen XM, Pollock CA. 2021. Metformin Attenuates Renal Fibrosis in a Mouse Model of Adenine-Induced Renal Injury Through Inhibiting TGF-beta1 Signaling Pathways. *Front Cell Dev Biol* **9**:603802. doi:10.3389/fcell.2021.603802

Zhao Q, Song W, Huang J, Wang D, Xu C. 2021. Metformin decreased myocardial fibrosis and apoptosis in hyperhomocysteinemia -induced cardiac hypertrophy. *CURR RES TRANSL MED* **69**:103270. doi:10.1016/j.retram.2020.103270

Zhao Q, Song W, Huang J, Wang D, Xu C. 2021. Metformin decreased myocardial fibrosis and apoptosis in hyperhomocysteinemia -induced cardiac hypertrophy. *CURR RES TRANSL MED* **69**:103270. doi:10.1016/j.retram.2020.103270

Zode GS, Sharma AB, Lin X, Searby CC, Bugge K, Kim GH, Clark AF, Sheffield VC. 2014.

535 Ocular-specific ER stress reduction rescues glaucoma in murine glucocorticoid-induced glaucoma. *J*
536 *CLIN INVEST* **124**:1956-1965. doi:10.1172/JCI69774

537

Figure legends

Figure 1. Topical ocular DEX induced OHT in mice. A. Elevated IOP in DEX-treated C57BL/6J mice was induced significantly at 3 weeks ($p < 0.01$). B. There was no significant change in the body weight of the DEX-treated group ($p > 0.05$). C. HE staining of OHT models. D. α-SMA and TGF-β staining in the representative OHT models. E-F. Quantification of α-SMA and TGF-β of the models. *$p < 0.05$, ns: non-significance, TM: trabecular meshwork, SC: Schlemm's canal, CB: cililary body.

Figure 2. Effect of metformin (MET) on OHT mice model. A. Experimental process overview. B. MET effectively reversed the IOP in steroid-induced OHT mice models. *$p < 0.05$, **$p < 0.01$, ns: non-significance.

Figure 3. MET decreased the expression of fibrotic markers in steroid-induced trabecular meshwork stiffening in mice. A-B. Representative images of HE (A) and fibrotic markers (B). C-D. Quantification of α-SMA of the models after 2 weeks (C) and 3 weeks (D) of MET treatment. E-F. Quantification of TGF-β of the models after 2 weeks (E) and 3 weeks (F) of MET treatment. G-H. Quantification of F-actin of the models after 2 weeks (G) and 3 weeks (H) of MET treatment. I-J. Quantification of fibronectin (FN) of the models after 2 weeks (I) and 3 weeks (J) of MET treatment. *$p < 0.05$, **$p < 0.01$, ns: non-significance. White arrows indicate the representative positive cells.

Figure 4. Low dose of metformin reversed the disarranged morphology of HTMC. A. HTMC were treated with metformin for 24 h with or without pre-treatment of tBHP for 1 h. Representative images of cell distribution and morphology photographed by inverted microscopy. B. The expression of myocilin after DEX treatment in HTMC. C-D. The relative HTMC viability after exposure to MET with different concentrations. Cell proliferation was measured using the CCK8 assay. E-F. The relative ROS levels were assayed via FCM and the results showed that metformin reduced the ROS production of HTMC induced by tBHP. **$p < 0.01$. *$p < 0.05$.

Figure 5. Metformin promoted the recovery of tBHP-induced cytoskeleton damages

(A) and activated intergrin/ROCK pathway (B) in HTMC. C. The quantitative protein levels of B. * $p < 0.05$ (comparison with the control), # $p < 0.05$ (comparison with the tBHP treated group).

Figure 6. Metformin partially normalized the damaged microfilaments of HTMC induced by tBHP. Red arrows indicate the representative microfilaments imaged by TEM.

Figure 1.

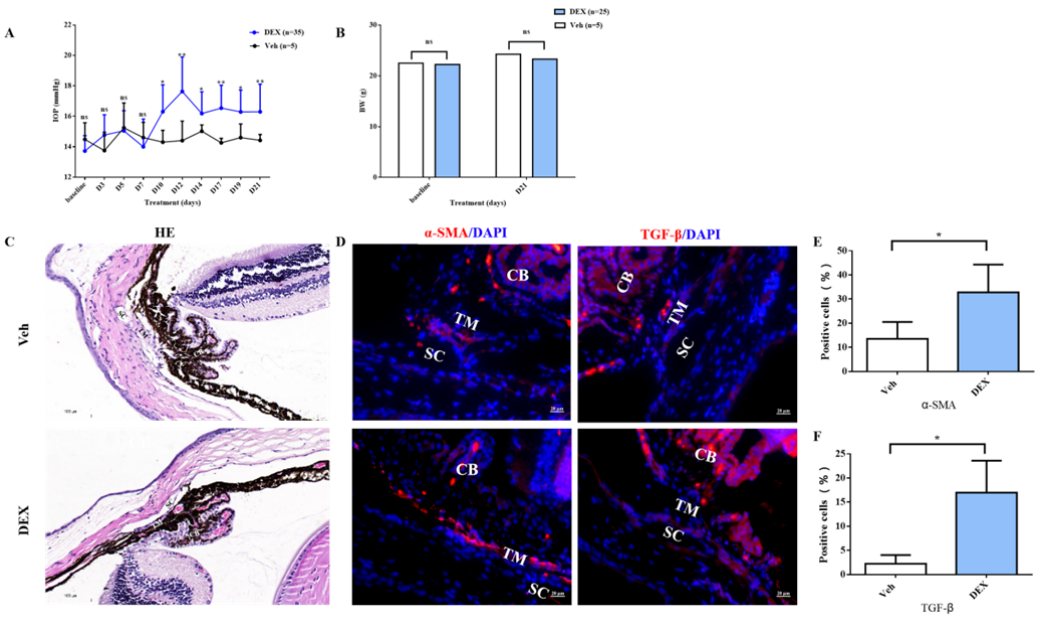

Figure 2.

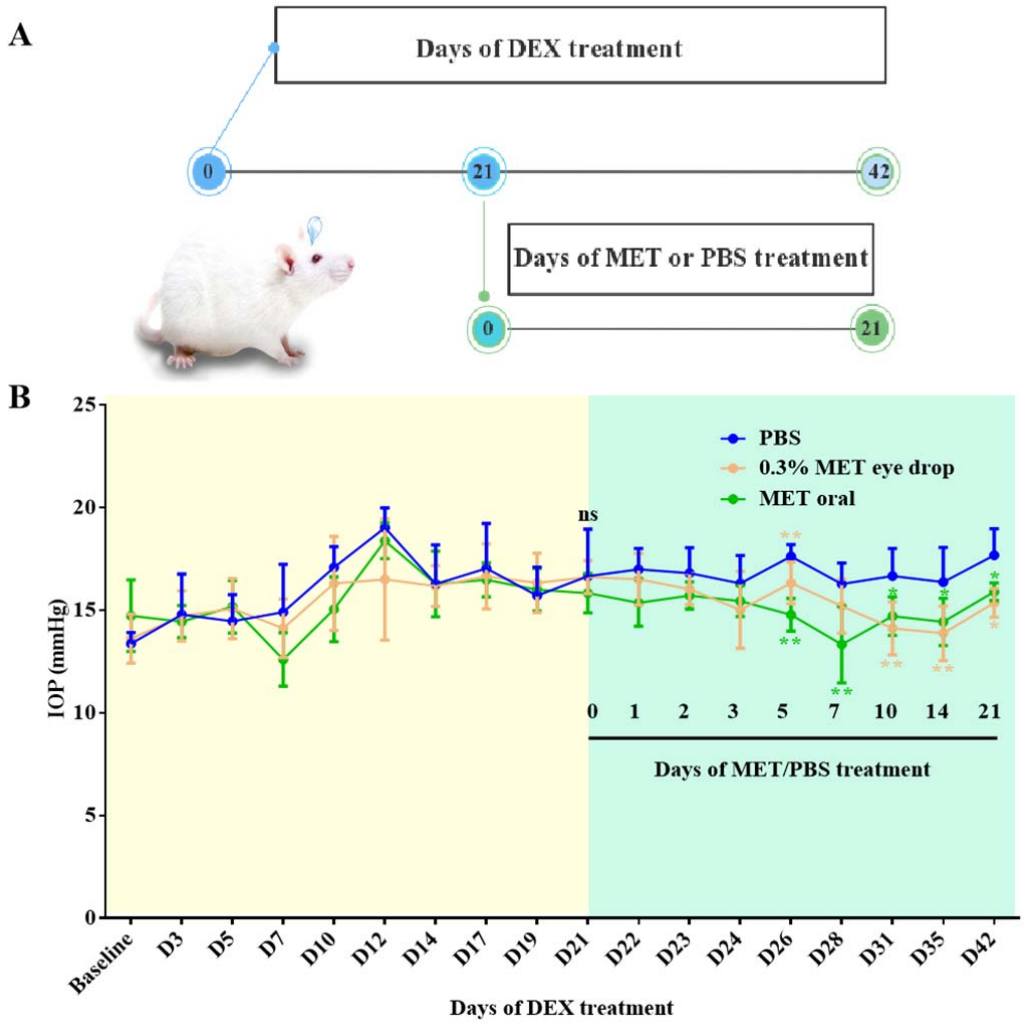

Figure 3.

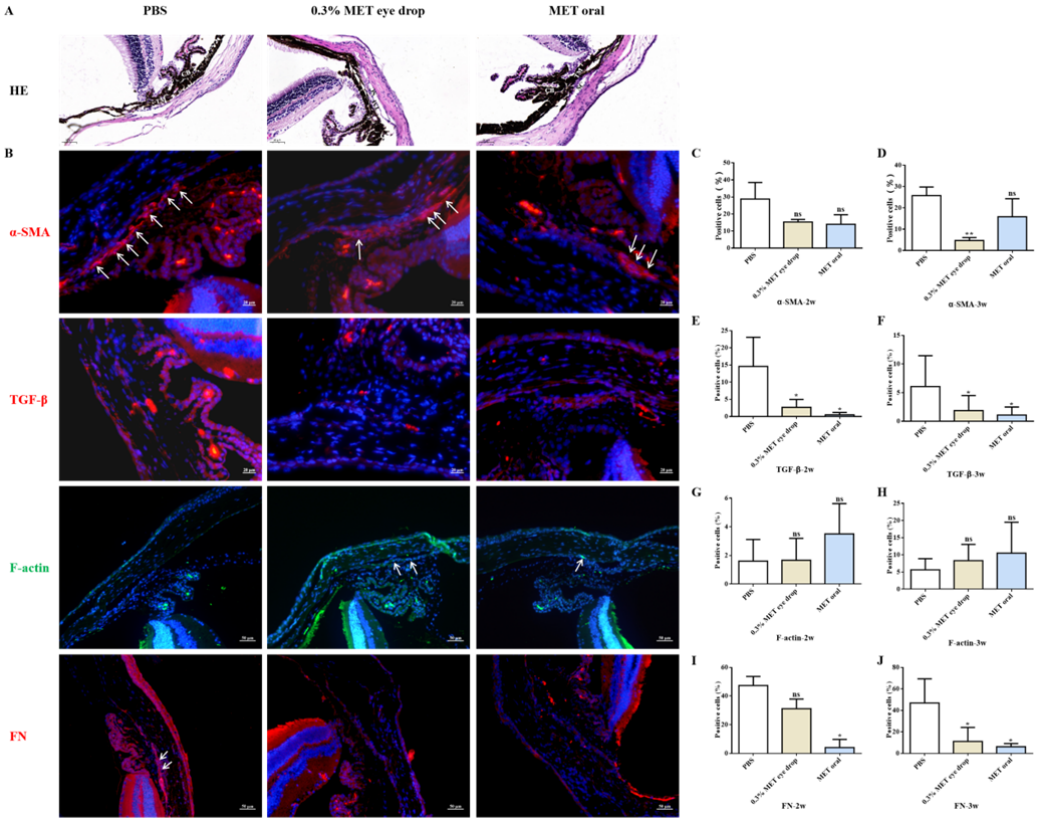

Figure 4.

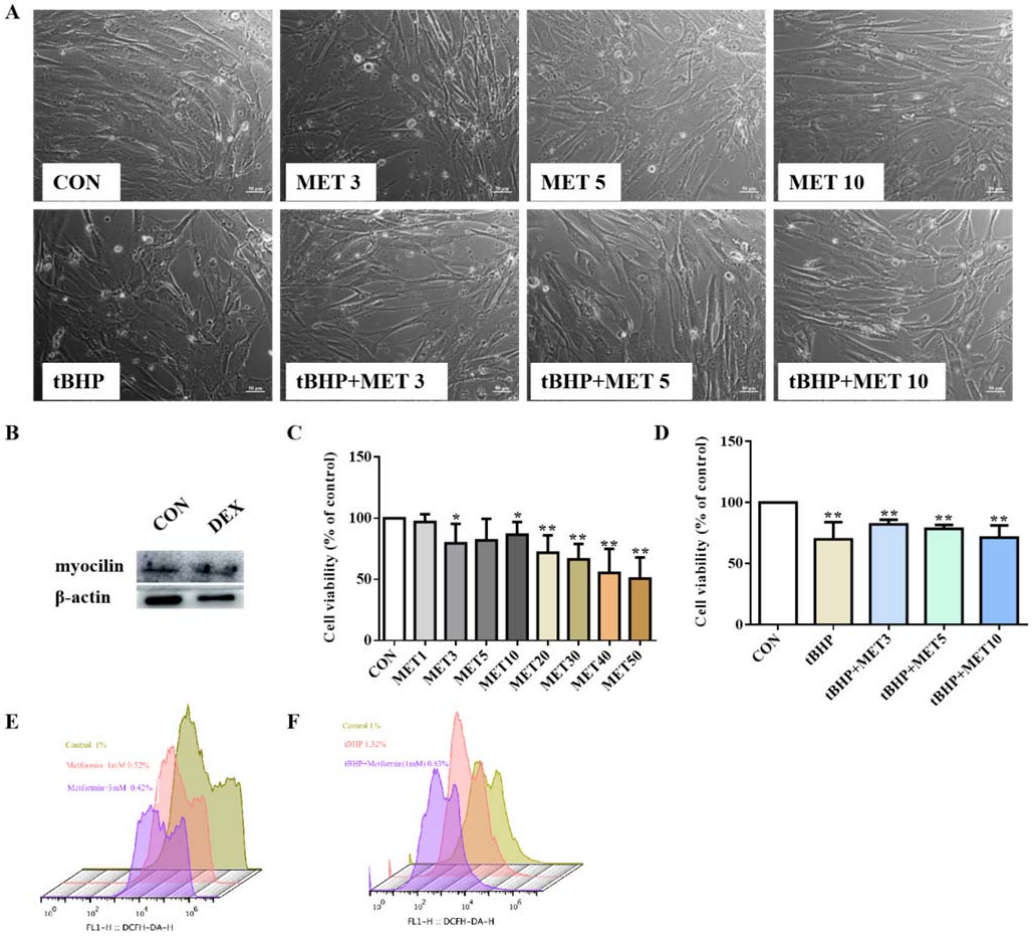

Figure 5.

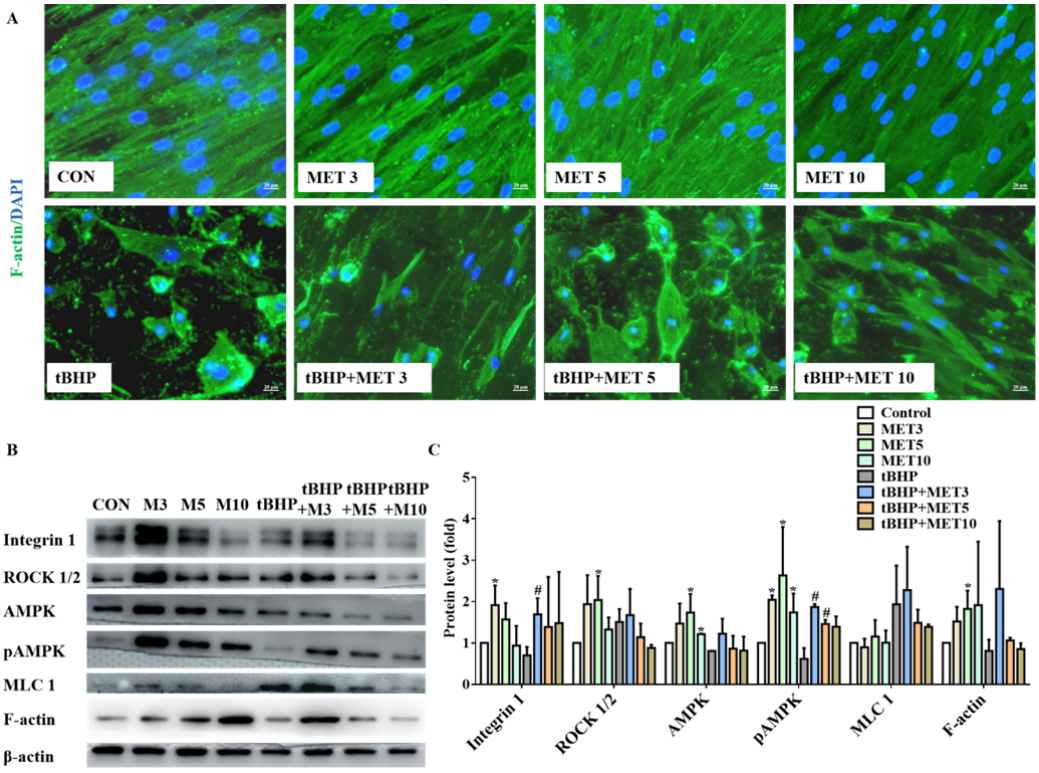

Figure 6.